A Spectroscopic Study on the Interactions of Porphyrin with G-Quadruplex DNAs†

Chunying Wei,‡ Guoqing Jia,‡ Jingli Yuan,§ Zhaochi Feng,‡ and Can Li*,‡

State Key Laboratory of Catalysis, Dalian Institute of Chemical Physics, Chinese Academy of Sciences, Dalian 116023, China, Laboratory of Analytical Chemistry, Dalian Institute of Chemical Physics, Chinese Academy of Sciences, Dalian 116023, China

Received November 17, 2005; Revised Manuscript Received February 24, 2006

ABSTRACT: Free-base porphyrin (5,10,15,20-tetrakis(1-methyl-4-pyridyl)-21H,23H-porphine) (H_2TMPyP4) has been shown to be an effective telomerase inhibitor by an in vitro assay. Here, we examined the interactions of the H_2TMPyP4 with three distinct G-quadruplex DNAs, the parallel-stranded $(TG_4T)4$, dimer-hairpin-folded $(G_4T_4G_4)2$, and monomer-folded $AG_3(T_2AG_3)_3$, by ultraviolet resonance Raman spectroscopy (UVRR), UV−vis absorption spectroscopy, fluorescence spectroscopy, and surface-enhanced Raman spectroscopy (SERS). The data obtained by the continuous variation titration method show that the binding stoichiometry of H_2TMPyP4/G-quadruplex is 2:1 for $(TG_4T)4$ and 4:1 for $(G_4T_4G_4)2$ or $AG_3(T_2AG_3)_3$. The results of SERS spectra, UV−vis absorption titration, and fluorescence emission spectra together with the binding stoichiometries reveal that two H_2TMPyP4 molecules are externally stacked at two ends of the parallel $(TG_4T)4$ G-quadruplex, whereas H_2TMPyP4 molecules can intercalate within their diagonal or lateral loop regions and intervals between two G-tetrads for $(G_4T_4G_4)2$ and $AG_3(T_2AG_3)_3$ G-quadruplexes. The binding of H_2TMPyP4 to $(TG_4T)4$ G-quadruplex results in the hypochromicity of the UV Raman signal of $(TG_4T)4$, indicating that the stacking effects between H_2TMPyP4 and DNA bases are significant. The Raman hyperchromicities and shifts are observed after the binding of H_2TMPyP4 to both $(G_4T_4G_4)2$ and $AG_3(T_2AG_3)_3$ G-quadruplexes. This indicates that the intercalative H_2TMPyP4 can lengthen the vertical distance between adjacent G-tetrads of $(G_4T_4G_4)2$ and $AG_3(T_2AG_3)_3$ and change their conformations. The present study provides new insights into the effect of H_2TMPyP4 binding on the structures of G-quadruplexes and also demonstrates that Raman spectroscopy is an ideal method for examining the interaction between drugs and G-quadruplexes.

Telomeric DNA consists of simple tandem repeats of guanine-rich DNA sequences, such as $(TTAGGG)_n$ in vertebrates, $(TTGGGG)_n$ in *Tetrahymena,* and $(TTTTGGGG)_n$ in *Oxytricha nova* (*1*, *2*). The extreme 3′ ends of eukaryotic telomeric DNA are single-stranded, which are able to form a variety of four-stranded structures known as G-quadruplexes in vitro based on a G-tetrad structure of four Hoogsteen-paired, coplanar guanines (Figure 1A) (*3*−*5*). Although there is no direct evidence of G-quadruplex structures in vivo, the potential role of G-quadruplexes in vivo has been highlighted with the recent development of chemotherapeutic strategies designed to stabilize telomeric ends as G-quadruplex structures using specific small molecules, which can destabilize telomere maintenance in tumor cells (*6*−*10*).

A number of G-quadruplex-binding compounds have been identified (*10*−*14*). Currently, porphyrin ligands are attracting considerable interest as potential telomerase inhibitors because of their low toxicity (*15*−*23*). In particular, the free-base porphyrin (5,10,15,20-tetrakis(1-methyl-4-pyridyl)-

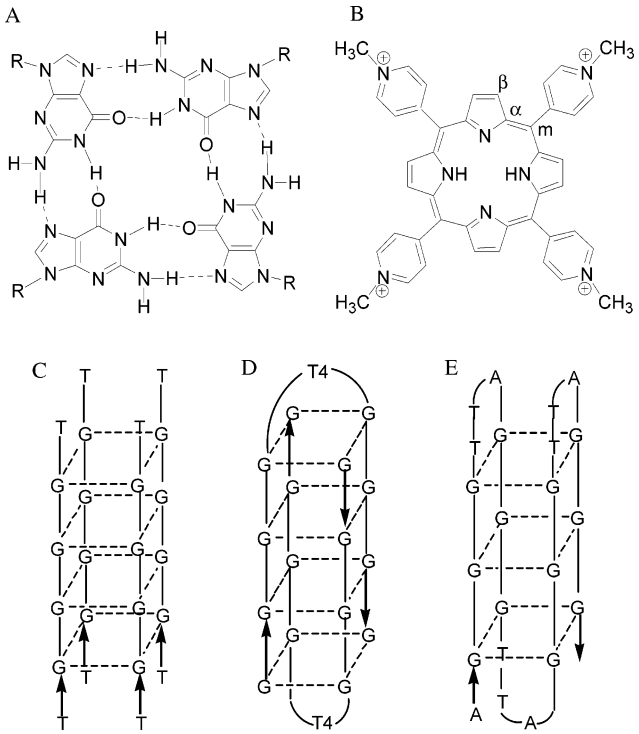

FIGURE 1: Structures of (A) a G-tetrad showing the Hoogsteen base pairing and (B) H_2TMPyP4 and schematic diagrams of (C) $(TG_4T)4$, (D) $(G_4T_4G_4)2$, and (E) $AG_3(T_2AG_3)_3$ G-quadruplexes in this study. Arrows denote 5′ → 3′ strand alignment for each DNA.

† This work was financially supported in part by The National Natural Science Foundation of China (20503029) and Scientific Research Innovation Foundation of The National Natural Science Foundation of China (20321303).

* To whom correspondence should be addressed. Telephone: 86-411-84379070. Fax: 86-411-84694447. E-mail: canli@dicp.ac.cn. Web site: http://www.canli.dicp.ac.cn.

‡ State Key Laboratory of Catalysis.

§ Laboratory of Analytical Chemistry.

10.1021/bi052356z CCC: $33.50
Published on Web 05/04/2006

21H,23H-porphine) (H_2TMPyP4)[1] (Figure 1B) has been shown to be an effective inhibitor of human telomerase by an in vitro assay in intact MCF7 human breast carcinoma cells (*23*).

However, there are still some controversies about the binding stoichiometries, exact modes, and binding sites of H_2TMPyP4 bound to G-quadruplexes. Two different G-quadruplex-binding modes have been proposed for H_2TMPyP4. One mode is the intercalation between adjacent G-tetrads. Haq and co-workers proposed that H_2TMPyP4 is intercalated in the center of the stack of G-tetrads in both parallel [$(T_4G_4)4$] and folding [$G_2T_2G_2TGTG_2T_2G_2$ and $AG_3(T_2AG_3)_3$] G-quadruplexes by isothermal titration calorimetry (ITC), UV−vis absorption spectrometry, and molecular-modeling methods (*16*). The stoichiometries correspond to the number of intervals between successive G-tetrad planes in each G-quadruplex. Using absorption spectra, circular dichroism (CD), and fluorescence energy-transfer methods, Anantha and co-workers also suggested that H_2TMPyP4 bind to the parallel $(T_4G_4)4$ G-quadruplex via the intercalative mode, but the binding stoichiometry is 1:1 (*22*). Another model assumed that H_2TMPyP4 binds to the parallel and antiparallel G-quarduplex structures through external stacking at the two ends (including loop regions) based on the spectroscopic methods, photocleavage experiments, and molecular dynamics calculations (*17*, *18*). As described above, the nature of the interaction between H_2TMPyP4 and G-quadruplexes has not been well-understood and the extensive and systematic investigation is necessary, particularly using molecular and electronic spectroscopic methods.

In the present study, using surface-enhanced Raman spectroscopy (SERS) and UV resonance Raman spectroscopy (UVRR), together with UV−vis absorption and fluorescence spectroscopy, we examined the interactions of H_2TMPyP4 with three G-quadruplex DNAs, $(TG_4T)4$, $(G_4T_4G_4)2$, and $AG_3(T_2AG_3)_3$, under conditions that favor self-assembly to their respective inter- or intramolecular G-quadruplexes (parts C−E of Figure 1). To the best of our knowledge, the SERS and UVRR of the H_2TMPyP4 bound to G-quadruplexes are reported here for the first time. Our study shows the substantial differences in the stoichiometric ratio and stack position when compared with previous studies. The H_2TMPyP4 molecules bind to the parallel-stranded $(TG_4T)4$ by end stacking with a 2:1 binding stoichiometric ratio, which is 4:1 for the H_2TMPyP4 bound to both $(G_4T_4G_4)2$ and $AG_3(T_2AG_3)_3$ G-quadruplexes, involving a mixed mode of the end stacking in loop regions and intercalation between G-tetrads. H_2TMPyP4 binding to the two ends of the parallel-stranded $(TG_4T)4$ G-quadruplex can effectively stack with G-tetrads, whereas the intercalated H_2TMPyP4 can lengthen the distance between the G-tetrads and has a significant effect on the structures of $(G_4T_4G_4)2$ and $AG_3(T_2AG_3)_3$ G-quadruplexes.

MATERIALS AND METHODS

Materials. H_2TMPyP4 was purchased in the form of tetra-*p*-tosylate salt from Tokyo Kasei Kogyo Co., Ltd. (Japan). Concentrated H_2TMPyP4 solution in distilled deionized water was stored in the dark at −20 °C to prevent photodegradation. Before experiments, the concentrated H_2TMPyP4 was diluted to a buffer solution composed of 10 mM Tris-HCl, 1 mM Na_2EDTA, and 100 mM KCl or 100 mM NaCl (as required) at pH 7.5. The concentration of H_2TMPyP4 was determined by measuring the absorbance at 424 nm with an extinction coefficient of 2.26×10^5 M^{-1} cm^{-1} (*24*).

The DNA oligonucleotides TG_4T, $G_4T_4G_4$, and $AG_3(T_2AG_3)_3$ were purchased from the SBS Genetech Co., Ltd. (China) in a HPLC-purified form. Single-strand concentrations were determined by measuring the absorbance at 260 nm at a high temperature using a JASC spectrophotometer. Single-strand extinction coefficients were calculated from mono- and dinucleotide data by a nearest-neighbor approximation method (*25*), using extinction coefficients at 260 nm of 57 800, 115 200, and 228 500 M^{-1} cm^{-1} for TG_4T, $G_4T_4G_4$, and $AG_3(T_2AG_3)_3$, respectively. The formation of intra- and intermolecular G-quadruplexes was carried out as follows: the oligonucleotide samples, dissolved in a buffer solution consisting of 10 mM Tris-HCl, 1 mM Na_2EDTA, and 100 mM KCl for $(TG_4T)4$ or 100 mM NaCl for both $(G_4T_4G_4)2$ and $AG_3(T_2AG_3)_3$ at pH 7.5, were heated to 90 °C for 5 min, gently cooled to room temperature, and then incubated at 4 °C overnight.

UV−Vis Absorption Titration Experiments. Absorption spectra were measured on a Jasco-V-550 UV−vis double-beam spectrophotometer with a 1 cm path-length quarter cell. The reference solution was 10 mM Tris-HCl, 1 mM Na_2EDTA, and 100 mM KCl (or 100 mM NaCl) at pH 7.5. UV−vis absorption titrations were carried out by the stepwise addition of G-quadruplex solutions to a cell containing 5 μM H_2TMPyP4. Absorption spectra were recorded in the 350−500 nm range at room temperature. The titration was terminated when the wavelength and intensity of the absorption band for H_2TMPyP4 did not change any more upon three successive additions of G-quadruplexes.

In the Scatchard equation, $r/C_f = K(n - r)$, where r is the number of moles of H_2TMPyP4 bound to 1 mol of G-quadruplex (C_b/C_{DNA}), n is the number of equivalent binding sites, and K is the affinities of ligands for those sites (*22*, *26*, *27*). The concentrations of free H_2TMPyP4 (C_f) and bound H_2TMPyP4 (C_b) are calculated using $C_f = C(1 - \alpha)$ and $C_b = C - C_f$, respectively, where C is the total porphyrin concentration (5 μM). The fraction of bound H_2TMPyP4 (α) was calculated using the equation, $\alpha = (A_f - A)/(A_f - A_b)$ (*21*), where A_f and A_b are the absorbance of the free and fully bound H_2TMPyP4 at the Soret maximum (422 nm) of H_2TMPyP4, respectively, and A is the absorbance (422 nm) at any given point during the titration.

The percent hypochromicity of the Soret band of H_2TMPyP4 can be calculated using the percent hypochormicity $= [(\epsilon_f - \epsilon_b)/\epsilon_f] \times 100$, where $\epsilon_b = A_b/C_b$ (*21*, *22*).

Continuous Variation Analysis. Stock solutions of 30 μM H_2TMPyP4 and 30 μM G-quadruplexes [$(TG_4T)4$, $(G_4T_4G_4)2$, and $AG_3(T_2AG_3)_3$] were prepared in their respective buffer solutions. Two series of solutions were used for the experiments: one with a varying mole fraction of H_2TMPyP4 and G-quadruplex and another with varying concentrations of H_2TMPyP4, while the sum of the H_2TMPyP4 and G-quadruplex concentration was kept at 30 μM. Absorption difference spectra were collected from 350 to 500 nm with

[1] Abbreviations: H_2TMPyP4, (5,10,15,20-tetrakis(1-methyl-4-pyridyl)-21H,23H-porphine); ITC, isothermal titration calorimetry; UVRR, ultraviolet resonance Raman spectroscopy; SERS, surface-enhanced Raman spectroscopy; dG, deoxyguanosine; CD, circular dichroism; EB, ethidium bromide.

a 1 cm path-length quartz cell. For each spectrum collected, the H_2TMPyP4 solution without an olignucleotide was placed in the reference compartment and the corresponding H_2TMPyP4 solution with an oligonucleotide was placed in the sample compartment. Cells were cleaned with concentrated HCl between measurements to remove all traces of H_2TMPyP4 that easily deposits on the quartz cell.

The difference in the maximum absorbance values at two wavelengths was plotted versus the H_2TMPyP4 mole fraction to generate a Job plot (*21*, *28*, *29*), which corresponds to the absorbance difference values between 443 and 420 nm for both $(TG_4T)4$ and $AG_3(T_2AG_3)_3$ and 440 and 420 nm for $(G_4T_4G_4)2$. Linear regression analysis of the data was performed in the software of Origin 7.0.

Emission Spectroscopy. Fluorescence emission spectra were measured at room temperature on the Perkin−Elmer LS 50B spectrofluorometer with a 1 cm path-length quartz cuvette. Emission spectra were obtained for 4 μM H_2TMPyP4 and the mixtures of 4 μM H_2TMPyP4 with 20 μM G-quadruplexes. The excitation wavelength was 433 nm, which is close to the isosbestic point of the absorption spectra, and the emission spectrum was collected from 600 to 800 nm. Excitation and emission slits were set at 10 and 5 nm, respectively.

SERS. Ag colloids were prepared by reducing $AgNO_3$ with $NaBH_4$ according to the reported method (*30*). The Ag colloid/H_2TMPyP4 (or Ag colloid/G-quadruplex) SERS-active systems were prepared by mixing equal volume of the H_2TMPyP4 (or G-quadruplex) solution with the Ag colloid in buffer solution containing either 100 mM KCl or 100 mM NaCl to obtain the desired H_2TMPyP4 or G-quadruplex concentrations. In the H_2TMPyP4/G-quadruplex complex experiments, the solution of G-quadruplex was mixed with the H_2TMPyP4 solution at a G-quadruplex/porphyrin ratio of 25, then an equal volume of the mixed solution was fully mixed with the Ag colloid, and the spectrum was immediately measured at room temperature. The final concentrations of H_2TMPyP4 and G-quadruplexes in all of the SERS-active systems were 1 and 25 μM, respectively.

SERS spectra were recorded using a Coherent DPSS 532 model 200 532 nm single-frequency laser, which is a diode-pumped, frequency-doubled Nd/YAG laser. The SERS signal was collected with conventional 90° geometry. The spectra were dispersed by a Jobin-Yvon U1000 scanning double monochromator with a spectral resolution of 4 cm^{-1}. A water-cooled RCA C31034A photomultiplier tube was used for detection, with photocounting electronics for data acquisition. A micropositionable quadrant cell holder was used for accurate and precise positioning of a 6 mm cuvette. Each spectrum took about 15 min to acquire.

UVRR. Samples of $(TG_4T)4$, $(G_4T_4G_4)2$, or $AG_3(T_2AG_3)_3$ with the G-quadruplex concentration at 25 μM were prepared in buffers containing 10 mM Tris-HCl, 1 mM Na_2EDTA, 25 mM Na_2SO_4, and 100 mM KCl or 100 mM NaCl diluted with a 30 mg/mL stock solution. Na_2SO_4 (981 cm^{-1}) in buffer was chosen as the intensity internal standard.

The UVRR was carried out on a T64000 triple-stage spectrometer of Jobin-Yvon S. A. equipped with three 2400 grooves mm^{-1} gratings and a specially coated UV-sensitive CCD detector. A 244 nm line from a Coherent Innova 300 FRED laser was used as the excitation source. The spectra were recorded in the stainless-steel cell using a 90° geometry, with a laser power of less than 1 mW on the sample to avoid thermal damage of the sample. Each spectrum was collected for 50 s; two spectra were accumulated to increase the signal-to-noise ratio. No photochemical damage was observed for all samples as judged by the absence of transient and irreversible changes in UVRR spectra within time of data collection. Raman frequencies were calibrated using the spectrum of Teflon.

RESULTS

Binding Modes of H_2TMPyP4 to G-Quadruplexes. UV−vis absorption is frequently used to investigate the DNA-binding behavior of a ligand. In this study, we examined the binding of H_2TMPyP4 to $(TG_4T)4$, $(G_4T_4G_4)2$, and $AG_3(T_2AG_3)_3$ G-quadruplexes by a UV−vis absorption titration experiment.

Figure 2 presents the changes of the absorption spectra of H_2TMPyP4 with titrations of $(TG_4T)4$, $(G_4T_4G_4)2$, and $AG_3(T_2AG_3)_3$ G-quadruplexes, respectively. The changes in the Soret band of H_2TMPyP4 after fully binding to G-quadruplexes are summarized in Table 1.

Both $(G_4T_4G_4)2$ and $AG_3(T_2AG_3)_3$ G-quadruplexes produce the larger red shifts and greater degrees of hypochromicities in the Soret band of H_2TMPyP4 (422 nm) compared with the $(TG_4T)4$ G-quadruplex. A tightly isosbestic point (433 nm) is observed for $(TG_4T)4$ and $AG_3(T_2AG_3)_3$. Conversely, for $(G_4T_4G_4)2$, near the end of titration, a slight deviation from the isosbestic point is observed, which suggests that the binding of H_2TMPyP4 to $(G_4T_4G_4)2$ be composed of several steps.

Furthermore, fluorescence spectra can reflect the information about the changes of the local environment of the chromophore and, therefore, can probe the interaction of the fluorophore with its environment. Here, we examined the interactions of H_2TMPyP4 with the three G-quadruplexes by fluorescence spectroscopy (Figure 3).

As shown in Figure 3, the interactions of H_2TMPyP4 with G-quadruplexes are evidently reflected in the shape and intensity of the emission spectrum of H_2TMPyP4. A significant increase in the emission intensity can be observed at a fixed H_2TMPyP4 concentration in the presence of a large excess of G-quadruplexes. The emission intensities of H_2TMPyP4 associated with $(G_4T_4G_4)2$ and $AG_3(T_2AG_3)_3$ are larger by about 2.5 and 1.5 times that of H_2TMPyP4 associated with $(TG_4T)4$, respectively, and the emission maxima are at 660 and 720 nm for H_2TMPyP4/$(TG_4T)4$, 660 and 723 nm for H_2TMPyP4/$AG_3(T_2AG_3)_3$, and 655 and 720 nm for H_2TMPyP4/$(G_4T_4G_4)2$, respectively. These changes of the emission spectra of H_2TMPyP4 indicate the change of the local environment of H_2TMPyP4 bound to the G-quadruplexes.

Binding Stoichiometric Ratios of H_2TMPyP4 to G-Quadruplexes. The Scatchard analysis is a useful way to treat the binding data quantitatively, which can determine the numbers of equivalent binding sites and affinities of ligands for those sites (*21*, *31*). However, it was found that the Scatchard plots produced from the UV−vis absorption titration are nonlinear (Figure 4). Deviations from linearity may arise from the unequal association constants of H_2TMPyP4 for the different binding sites in G-quadruplexes.

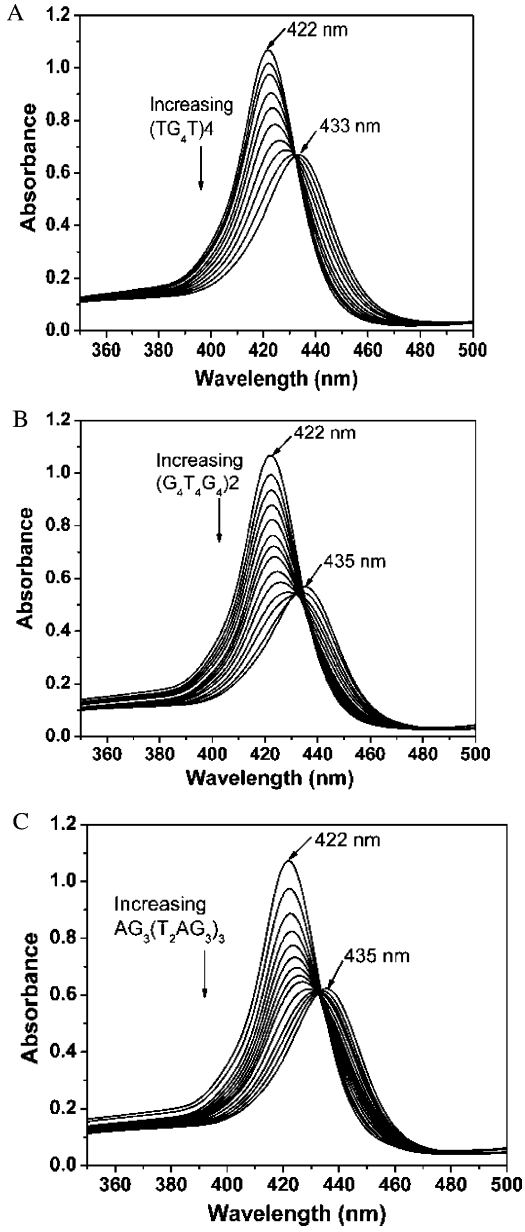

FIGURE 2: UV−vis absorption titration spectra of 5 μM H_2TMPyP4 with (A) $(TG_4T)4$, (B) $(G_4T_4G_4)2$, and (C) $AG_3(T_2AG_3)_3$ G-quadruplexes in 10 mM Tris-HCl, 1 mM Na_2EDTA, and 100 mM KCl or 100 mM NaCl buffer at pH 7.5. Additions range from 0 to 9.5, 0 to 4.5, and 0 to 4.8 μM for $(TG_4T)4$, $(G_4T_4G_4)2$, and $AG_3(T_2AG_3)_3$, respectively.

Table 1: UV−Vis Absorbance Titration Parameters for H_2TMPyP4 with G-Quadruplexes

G-quadruplex	[G-quadruplex][a] (μM)	Soret band shift (nm)	percent hypochromicity[b]
$(TG_4T)4$	9.5	11	56.7
$(G_4T_4G_4)2$	4.5	13	62.8
$AG_3(T_2AG_3)_3$	4.8	13	61.1

[a] [G-quadruplex] is the concentration of the G-quadruplexes at the end of titration. [b] $\epsilon_b = 9.8 \pm 0.04 \times 10^4$, $8.5 \pm 0.17 \times 10^4$, and $8.7 \pm 0.11 \times 10^4$ M^{-1} cm^{-1} for $(TG_4T)4$, $(G_4T_4G_4)2$, and $AG_3(T_2AG_3)_3$, respectively.

In an attempt to determine the number of ligand-binding sites, data points at lower *r* values between 0.73 and 1.27 for $(TG_4T)4$, 1.58 and 2.50 for $(G_4T_4G_4)2$, and 1.16 and 3.04 for $AG_3(T_2AG_3)_3$ were fit to the Scatchard model and the

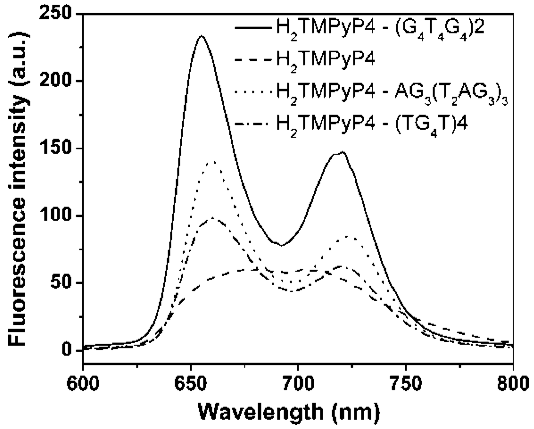

FIGURE 3: Fluorescence emission spectra of 4 μM H_2TMPyP4 and its complexes with $(TG_4T)4$, $AG_3(T_2AG_3)3$, and $(G_4T_4G_4)2$ G-quadruplexes at 20 μM. All solutions contain 10 mM Tris-HCl, 1 mM Na_2EDTA, and 100 mM KCl or 100 mM NaCl at pH 7.5.

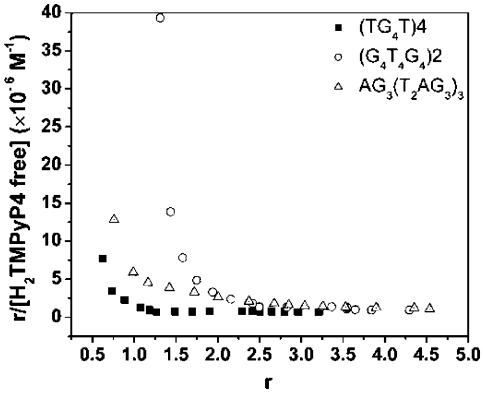

FIGURE 4: Scatchard plots for H_2TMPyP4 with $(TG_4T)4$, $(G_4T_4G_4)2$, and $AG_3(T_2AG_3)_3$ G-quadruplexes.

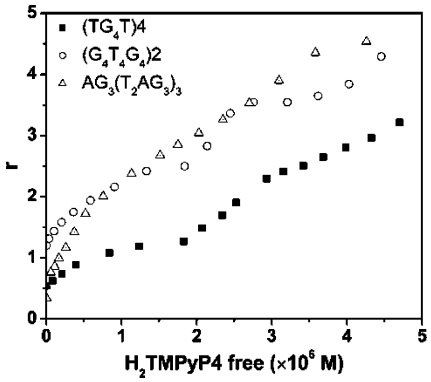

FIGURE 5: Plots of *r* (moles of bound H_2TMPyP4/1 mol of G-quadruplexes) versus $[H_2TMPyP4]_{free}$ for the absorption titrations of $[H_2TMPyP4]_{free}$ with $(TG_4T)4$, $(G_4T_4G_4)2$, and $AG_3(T_2AG_3)_3$ G-quadruplexes.

fitting gives *n* values of 1.7 for $(TG_4T)4$, 3.0 for $(G_4T_4G_4)2$, and 3.6 for $AG_3(T_2AG_3)_3$, respectively.

Rearrangement of the Scatchard equation yields another equation, i.e., $r = (nKC_f)/(1 + KC_f)$, which is the Direct plot. According to this equation, a plot of *r* versus the free ligand concentration should yield a hyperbola that can be fit to obtain the numbers of ligand-binding sites. Our plots of *r* versus the free H_2TMPyP4 concentration (given in Figure 5) are sigmoidal, especially for $(TG_4T)4$ and $(G_4T_4G_4)2$ G-quadruplexes. The sigmoidal shape of plots indicates that the binding of H_2TMPyP4 to three G-quadruplexes is

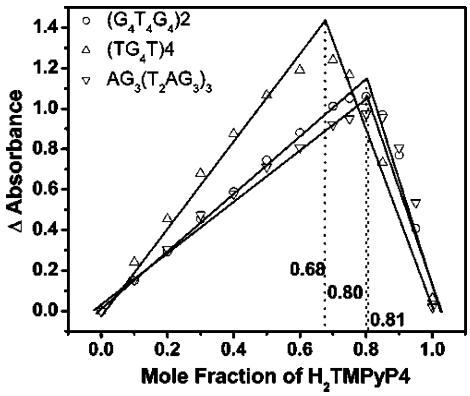

FIGURE 6: Job plots for the binding of H_2TMPyP4 to $(TG_4T)4$, $(G_4T_4G_4)2$, and $AG_3(T_2AG_3)_3$ G-quadruplexes in 10 mM Tris-HCl, 1 mM Na_2EDTA, and 100 mM KCl or 100 mM NaCl buffer at pH 7.5.

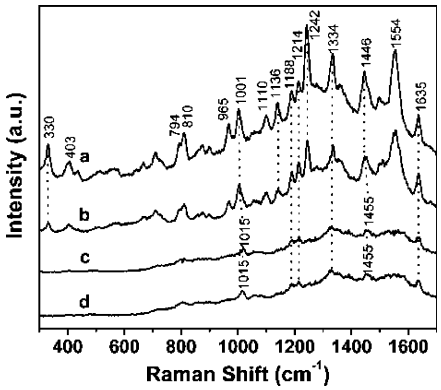

FIGURE 7: SERS spectra (300−1700 cm^{-1}) of (a) H_2TMPyP4 at 1 μM, (b) H_2TMPyP4-$(TG_4T)4$, (c) H_2TMPyP4-$AG_3(T_2AG_3)_3$, and (d) H_2TMPyP4-$(G_4T_4G_4)2$ complexes in buffer solution containing 10 mM Tris-HCl, 1 mM Na_2EDTA, and 100 mM KCl or 100 mM NaCl at pH 7.5. The molar ratio of G-quadruplex/H_2TMPyP4 is 25:1.

cooperative and means that the Direct plot is not suitable for evaluating the binding of H_2TMPyP4 to these G-quadruplexes.

To further identify and get exact numbers of ligand-binding sites, the method of continuous variation analysis (Job plot) was used. The points of the intersection of two fit lines in the Job plots (Figure 6) for the complexes of H_2TMPyP4 with $(TG_4T)4$, $(G_4T_4G_4)2$, and $AG_3(T_2AG_3)_3$ are 0.68, 0.80, and 0.81, corresponding to H_2TMPyP4/G-quadruplex stoichiometric ratios of 2.1:1, 4.0:1, and 4.2:1, respectively. The difference spectra, used to produce the Job plots in Figure 6, are available from the Supporting Information.

Binding Sites of H_2TMPyP4 to G-Quadruplexes. SERS is a powerful tool for the study of the interactions of the drugs, especially fluorescence molecules, with biomacromolecules at very low concentrations. The metal colloids can be adapted for the application in the study of biological objects, because they do not modify to a great extent the structures of biological molecules adsorbed on their surface (*32*). To further clarify the binding modes and sites of H_2TMPyP4 to G-quadruplexes, SERS spectra were measured.

The SERS spectrum of H_2TMPyP4 is shown in curve a in Figure 7. Table 2 summarized the main SERS bands of H_2TMPyP4 and their assignments. When displacing KCl with NaCl in buffer solution, the SERS spectrum of H_2TMPyP4 is hardly changed (spectrum not shown). The $NaBH_4$-reduced silver colloids have the negative charge on their surface, which repulses the adsorption of negative-charged DNA molecules, and therefore, none of three G-quadruplexes at 25 μM gives a SERS signal (spectrum not shown).

Table 2: Raman Frequencies and Assignments for H_2TMPyP4[a]

Raman shift (cm^{-1})	assignments[b]	Raman shift (cm^{-1})	assignments[b]
330	δ (por)	1188	δ (pyr), ν (N^+-CH_3)
403	δ (por) + ν (Ag−N)	1214	δ (pyr), ν ($N-C_\alpha$)
810	pyr ν (N^+-CH_3)	1242	ν (C_m-pyr)
	δ_s (por)	1334	ν_s ($N-C_\alpha$)
965	ν ($C_\alpha-C_\beta$)	1446	ν_s ($C_\alpha-C_\beta$)
1001	ν (C_m-C_α)	1554	ν ($C_\beta-C_\beta$)
1110	δ_s ($C_\beta-$H)	1635	δ (pyr)
1136	ν ($C_\alpha-$N)		

[a] Band assignments are according to refs *51*−*57*. [b] Abbreviations: ν, stretching mode; δ, bending mode; s, symmetric mode; pyr, *N*-methylpyridinium; por, porphyrin core.

Curve b in Figure 7 shows the SERS spectrum of a complex of H_2TMPyP4 at 1 μM with excess $(TG_4T)4$ at 25 μM. At this stoichiometric ratio, virtually all of H_2TMPyP4 molecules are bound to $(TG_4T)4$. Raman intensities of H_2TMPyP4 while interacted with $(TG_4T)4$ at 1188, 1214, and 1635 cm^{-1} have almost no changes, implying that these bands are insensitive to the interactions of H_2TMPyP4 with $(TG_4T)4$. However, significant decreases of relative intensities of bands at 330, 1136, and 1242 cm^{-1} and slight decreases of other bands are observed for the complex. This indicates the decrease of the amount of H_2TMPyP4 adsorbed on colloids accompanied by $(TG_4T)4$ binding.

Curves c and d in Figure 7 show the SERS spectra of 1 μM H_2TMPyP4 complexed with excess $AG_3(T_2AG_3)_3$ and $(G_4T_4G_4)2$ (25 μM), respectively. SERS spectra of both complexes are quite similar to each other but very different from that of the H_2TMPyP4/$(TG_4T)4$ complex. Most bands of the H_2TMPyP4/$AG_3(T_2AG_3)_3$ and H_2TMPyP4/$(G_4T_4G_4)2$ complexes disappear, and the bands at 1001 and 1446 cm^{-1} shift to 1015 and 1455 cm^{-1}, respectively. These results show that the interactions of H_2TMPyP4 with $AG_3(T_2AG_3)_3$ and $(G_4T_4G_4)2$ G-quadruplexes can largely reduce the amount of H_2TMPyP4 adsorbed on Ag colloids.

Effect of H_2TMPyP4 on the Structures of G-Quadruplexes. UVRR can selectively enhance the Raman intensities of the bands attributed to the given chromophores and has been used extensively to study the structure and bonding of biomacromolecules such as protein and nucleic acids (*33*, *34*). In an attempt to investigate the effect of ligand binding on the base stacking of G-quadruplexes, we carried out UVRR studies on the interactions of H_2TMPyP4 with G-quadruplex DNAs using a 244 nm line that is in the absorption region of the DNA and can selectively enhance the Raman intensity of DNA bases.

Figure 8 shows UVRR spectra of three G-quadruplexes together with their complexes with H_2TMPyP4 in the different molar ratios and their Raman difference spectra. The characteristic Raman band at 981 cm^{-1} of SO_4^{2-} is used as an internal standard reference band to normalize the intensity of the Raman spectra. UVRR bands of G-quadruplexes and their assignments are summarized in Table 3.

Figure 8A shows UVRR spectra of $(TG_4T)4$ at 25 μM and its complex with H_2TMPyP4 in the molar ratios of

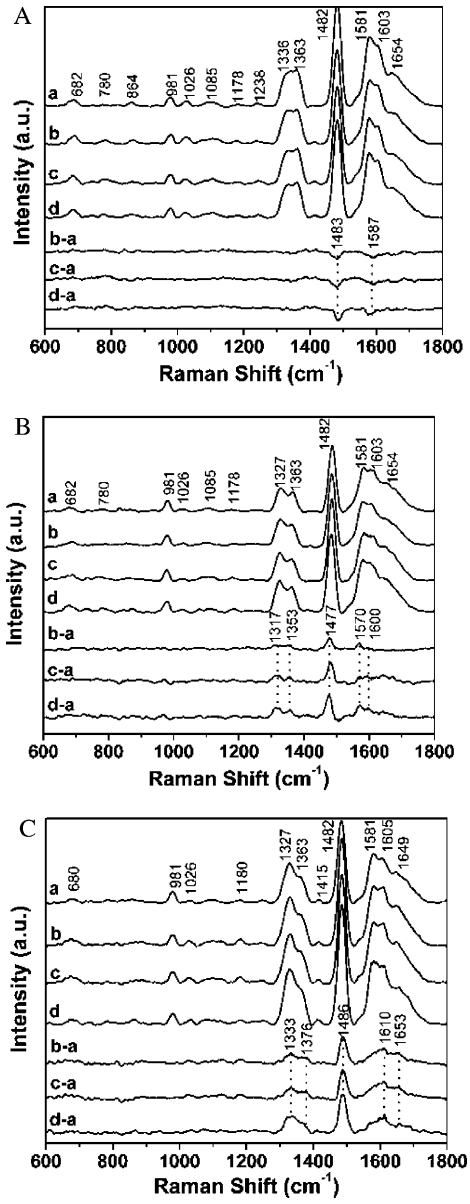

FIGURE 8: UVRR spectra (600−1800 cm^{-1}) of G-quadruplexes (A) $(TG_4T)4$, (B) $(G_4T_4G_4)2$, and (C) $AG_3(T_2AG_3)_3$ as well as their complexes with $H_2TMPyP4$ in the different molar ratios in buffer solution containing 10 mM Tris-HCl, 1 mM Na_2EDTA, and 100 mM KCl or 100 mM NaCl at pH 7.5. The molar ratios of G-quadruplex/$H_2TMPyP4$ are 0, 5:1, 1:1, and 1:2 for curves a, b, c, and d, respectively. Curves b-a, c-a, and d-a are the Raman difference spectra ($H_2TMPyP4$/G-quadruplex complexes−G-quadruplexes).

G-quadruplex/$H_2TMPyP4$ at 5:1, 1:1, and 1:2. Under these conditions, no Raman signal of $H_2TMPyP4$ is observed. The spectrum (curve a in Figure 8A) exhibits the marker bands of the parallel $(TG_4T)4$ G-quadruplex at 682, 1336, and 1482 cm^{-1}. The peaks at 682 and 1336 cm^{-1} identify deoxyguanosine (dG) residues in a C2′-endo/anti conformation (*35*). In addition, the Raman marker at 1482 cm^{-1} is sensitive to Hoogsteen hydrogen bonding at the guanine N7 site and constitutes a definitive probe of G-quadruplex formation (*36*). Curves a in parts B and C of Figure 8 show the UVRR spectra of $(G_4T_4G_4)2$ and $AG_3(T_2AG_3)_3$, respectively. Besides the bands at 682 and 1482 cm^{-1}, another marker band at 1327 cm^{-1} corresponding to dG in a C2′-endo/syn conformation appears (*37*); a similar Raman fingerprint was reported for $(G_4T_4G_4)2$ (*38*). These results indicate that $(TG_4T)4$ contains an anti dG conformation, but two different dG conformations (syn and anti) appear to coexist for $(G_4T_4G_4)2$ and $AG_3(T_2AG_3)_3$ in the buffer solution containing 100 mM NaCl. Therefore, $(TG_4T)4$ is a parallel-stranded G-quadruplex, and $(G_4T_4G_4)2$ and $AG_3(T_2AG_3)_3$ are in the form of folding antiparallel G-quadruplexes. Structures of G-quadruplexes are therefore consistent with the structures shown in Figure 1 and also entirely identical to those reported in the literature (*39*−*44*).

Table 3: UV Resonance Raman Bands of Telomeric DNA in H_2O Solution

bands (cm^{-1})	assignments[a]
680 (682)	dG C2′-endo/anti
780	bk OPO; dT
1026	dG
1085	dG
1178 (1180)	unpaired dT (N3)
1238	dT (N3)
1327	dG C2′-endo/syn
1336	dG C2′-endo/anti
1363	dG (N2), C2′-endo/anti
1482	dG N7 hydrogen bond
1581	dG N2H interbase hydrogen bond
1603 (1605)	dG N1H interbase hydrogen bond
1654 (1649)	dT C═O O6 hydrogen bond

[a] Band assignments are according to refs *35*−*38*.

Curves b−d in parts A−C of Figure 8 show UVRR spectra of the $H_2TMPyP4$/G-quadruplex complexes, and the corresponding difference spectra were computed by subtracting the Raman spectrum of the G-quadruplex from the Raman spectrum of their $H_2TMPyP4$/G-quadruplex complexes (curves b-a, c-a, and d-a in parts A−C of Figure 8). In the difference spectra, the negative peaks at 1483 and 1587 cm^{-1} are observed for the $H_2TMPyP4$/$(TG_4T)4$ complexes (Figure 8A) but some positive peaks are observed at 1317, 1353, 1477, 1570, and 1600 cm^{-1} for the $H_2TMPyP4$/$(G_4T_4G_4)2$ complex (Figure 8B) and at 1333, 1376, 1486, 1610, and 1653 cm^{-1} for the $H_2TMPyP4$/$AG_3(T_2AG_3)_3$ complex (Figure 8C). These negative and positive peaks in the difference spectra reflect the changes of the stacking interaction in the complexes. In addition, the shifts of peaks in the difference spectra are observed for the $H_2TMPyP4$/$(G_4T_4G_4)2$ and $H_2TMPyP4$/$AG_3(T_2AG_3)_3$ complexes relative to G-quadruplexes. This spectroscopic information indicates the conformational changes of G-quadruplexes.

DISCUSSION

Binding Modes of $H_2TMPyP4$ to G-Quadruplexes. The size and concentration of cations either Na^+ or K^+ in the buffer solution may affect the structures of G-quadruplexes, such as the orientation of sequential guanine and the conformation of the loop. Generally, there are only minor changes in the size of the G-quartet in Na^+ and K^+ forms of the parallel-stranded G-quadruplexes. Conversely, the folded G-quadruplexes present the diverse structures in buffer containing either Na^+ or K^+. In the case of dimer hairpin G-quadruplexes, the structures of $(G_4T_4G_4)2$ determined by NMR in the presence of either Na^+ or K^+ have diagonal loops at opposite ends of the quadruplex stem (*45*, *46*), whereas the X-ray crystallography structure of $(G_4T_4G_4)2$, with K^+ as the coordinated cation, has lateral loops at either end of a

G-quadruplex (*47*). In addition, there are two types of G-quartet structure formed by intramolecularly folding $AG_3(T_2AG_3)_3$, i.e., the crossover and chair types. The former type can be formed in the presence of Na^+ alone as well as in the presence of K^+ alone, while the latter has been observed only in the presence of K^+ (*48*). Furthermore, the crystal structure of the parallel G-quadruplex was also reported for $AG_3(T_2AG_3)_3$ in a buffer containing K^+ (*49*). On the other hand, it was reported that a high ion concentration in the solution is not favorable for the loop formation for dimer-hairpin- or monomer-folded quadruplexes (*5*).

To avoid the formation of the mixture of G-quadruplexes with the different conformation, we carefully choose the buffer solution that contains 100 mM K^+ for $(TG_4T)4$ and 100 mM Na^+ for both $AG_3(T_2AG_3)_3$ and $(G_4T_4G_4)2$. Under these conditions, $(TG_4T)4$ can form the stable parallel four-stranded G-quadruplex and $AG_3(T_2AG_3)_3$ can fold to form the monomer G-quadruplex, which contains one diagonal TTA loop, two lateral TTA loops, and three G-quartets (*41*), although $(G_4T_4G_4)2$ can form the dimer hairpin G-quadruplex with two diagonal TTA loops and four G-quartets (*43*). The conformations of these G-quadruplexes have been confirmed by UVRR spectra.

UV−vis absorption titration experiments show that the binding of $H_2TMPyP4$ to G-quadruplexes results in red shifts (11−13 nm) and large hypochromicities (56−62%) in the Soret band of $H_2TMPyP4$. Although the observed red shifts are smaller than the values (at least 15 nm) of the typical intercalated binding, the large hypochromicities are in the range of an intercalated binding (at least 35%). In fact, the red shifts ($\geq$15 nm) and hypochromicities ($\geq$35%) given for intercalative binding modes were determined for long pieces of duplex DNA (*24*), where end stacking is not significant. Previous results have also indicated this difference between duplexes and quadruplexes (*16*, *21*, *22*). Therefore, the hypochromicities and red shifts in the absorption spectra of $H_2TMPyP4$ suggest the intercalative (containing the end stacking) binding mode for these G-quadruplexes.

In comparison with the results reported by Haq and co-workers (*16*), a smaller red shift and larger hypochromicity are observed for the binding of $H_2TMPyP4$ to $AG_3(T_2AG_3)_3$. This difference may be due to the different buffer solutions because of the different ions, ionic strength, and pH values in the two buffers. It was reported that the increase of the ionic strength of the buffer results in the decrease of the hypochromicity for $H_2TMPyP4$ binding to calf thymus DNA (*44*). The ionic strength in our buffer solution is lower than that used by Haq and co-workers (*16*), which may illustrate the difference in the hypochromicity.

Fluorescence experiments further support the intercalative and external stacking binding modes proposed by the UV−vis absorption titration results. In comparison with the free $H_2TMPyP4$, one of the obvious spectral changes is the increase in the emission intensities for three H_2TMPyP_4/G-quadruplex complexes, which apparently depends upon the structures of G-quadruplexes. The emission intensity of $H_2TMPyP4/(TG_4T)4$ is the weakest among the three complexes, suggesting that $H_2TMPyP4$ be stacked at the ends of $(TG_4T)4$. Because the external stacking $H_2TMPyP4$ will be exposed to the solvent to a larger extent, the solvent quenching is more significant.

On the contrary, for the $H_2TMPyP4/(G_4T_4G_4)2$ and $H_2TMPyP4/AG_3(T_2AG_3)_3$ complexes, $H_2TMPyP4$ is intercalated in the loop regions and intervals between adjacent G-tetrads and the intercalative $H_2TMPyP4$ is well-protected from the solvent and presents a large increase in the emission intensity. The difference of the emission intensity between $H_2TMPyP4/(G_4T_4G_4)2$ and $H_2TMPyP4/AG_3(T_2AG_3)_3$ complexes may be ascribed to their different loop structures. $(G_4T_4G_4)2$ contains two equivalent central T_4 diagonal loops at the opposite ends, but $AG_3(T_2AG_3)_3$ has one central diagonal TTA loop at one end and two lateral TTA loops at another end. For the $H_2TMPyP4/AG_3(T_2AG_3)_3$ complex, when $H_2TMPyP4$ is bound to the lateral TTA loop region of the $AG_3(T_2AG_3)_3$ G-quadruplex, the porphyrin core is partly exposed to the solvent. However, in the case of the $H_2TMPyP4/(G_4T_4G_4)2$ complex, the bound $H_2TMPyP4$ can be well-buried in the T_4 loop of the diagonally crossed G-tetrad, resulting in the decrease in the possibility for the contact of the $H_2TMPyP4$ core with the solvent. Thus, the different hydrophobic environment surrounding $H_2TMPyP4$ may explain the difference in the fluorescence intensities.

Besides the emission intensity, the shape of the emission spectra also gives information of the interaction. First, the local solvent environment of the bound $H_2TMPyP4$ will be very different from that of the free $H_2TMPyP4$. It was reported that the Q(0,0) fluorescence band of $H_2TMPyP4$ can be shifted to a longer wavelength in water to overlap the Q(0,1) band (*50*); thus, a broad emission spectrum of $H_2TMPyP4$ in aqueous solution was observed. With different solvent environments, both Q(0,0) and Q(0,1) bands of $H_2TMPyP4$ may shift to the different wavelengths (*50*), and two separated bands near 660 and 720 nm were observed in the emission spectra of all complexes. The positions of the emission peaks consist of the maxima of the typical emission spectrum of intercalated $H_2TMPyP4$ species (*51*).

Additionally, the binding forces could impose the forced rotation of the *N*-methylpyridyl group, which may also change the shape and intensity of the emission spectrum of $H_2TMPyP4$ in the complexes. Because the rotation angle of the *N*-methylpyridyl group depends upon the structure of the G-quadruplex, it is reasonable to have the significant difference of the emission intensities for three H_2TMPyP_4/G-quadruplex complexes.

The SERS spectra also reveal the external stacking mode for the $H_2TMPyP4/(TG_4T)4$ complex and a mixed binding mode containing the external stacking and intercalation for both $H_2TMPyP4/(G_4T_4G_4)2$ and $H_2TMPyP4/AG_3(T_2AG_3)_3$ complexes. In comparison with free $H_2TMPyP4$, the SERS spectrum of the $H_2TMPyP4/(TG_4T)4$ complex only shows a small change, whereas the SERS signals of $H_2TMPyP4$ disappear upon its interaction with $(G_4T_4G_4)2$ and $AG_3(T_2AG_3)_3$. In terms of the short-range character of the Raman enhancement in a colloid system (*52*), the SERS quenching is interpreted in term of a loss of accessibility for $H_2TMPyP4$ to the Ag colloids. The results imply that the binding mode of $H_2TMPyP4$ for $(TG_4T)4$ is end-stacking because of the slightly decreased SERS signals. Instead, $H_2TMPyP4$ presents a typical intercalating mode in both $(G_4T_4G_4)2$ and $AG_3(T_2AG_3)_3$ G-quadruplexes, because the molecule is intercalated within the loops and G-tetrads and thus becomes undetectable by SERS.

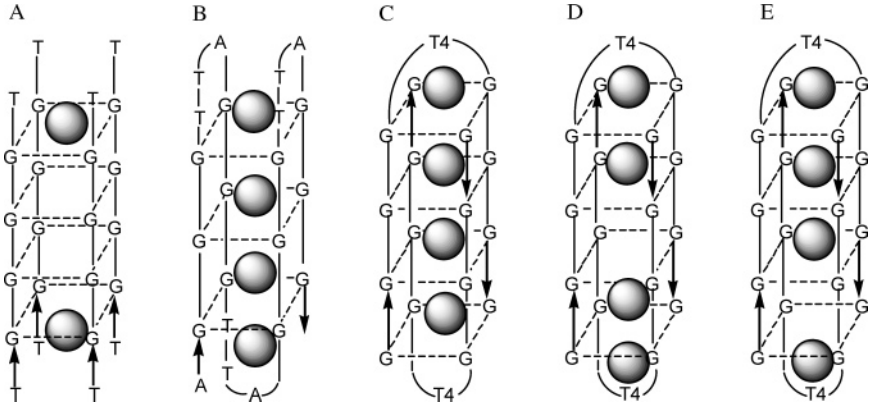

FIGURE 9: Proposed binding modes of H_2TMPyP4 to G-quadruplexes. (A) Two H_2TMPyP4 molecules are externally stacked at the opposite end of $(TG_4T)4$. (B) Two H_2TMPyP4 molecules are intercalated in the diagonal and lateral loops, and the other two H_2TMPyP4 are intercalated in the two intervals between adjacent G-tetrads of $AG_3(T_2AG_3)_3$. (C) One H_2TMPyP4 molecule binds to one of the T4 loop regions, and the other three H_2TMPyP4 molecules intercalate the three intervals between adjacent G-tetrads of $(G_4T_4G_4)2$ G-quadruplexes. (D and E) Two H_2TMPyP4 molecules stack in the two T4 loops, and the other two molecules bind to the two of three intervals of $(G_4T_4G_4)2$ G-quadruplexes. Balls denote the H_2TMPyP4 molecules, and arrows denote 5′ → 3′ strand alignment for each DNA.

The relative intensities and shifts of the bands in SERS spectra supply the information of the interaction of H_2TMPyP4 with G-quadruplexes. SERS bands at 1188, 1214, and 1653 cm^{-1} ascribed to *N*-methylpyridine are insensitive to the change of the interaction (*53*−*56*); therefore, their intensities are kept after the binding of H_2TMPyP4 to $(TG_4T)4$. The larger intensity decreases are observed at 330, 1136, and 1242 cm^{-1} compared with those of other bands for the H_2TMPyP4/$(TG_4T)4$ complex. The band at 330 cm^{-1} is mainly assigned to the bending vibration of H_2TMPyP4 and is the marker band of the free-base H_2TMPyP4 in the SERS-active system (*53*, *54*, *57*); the intensity decrease of this band is due to the decrease in the amount of free-base H_2TMPyP4 molecules surrounding Ag colloids after the interaction between H_2TMPyP4 and the $(TG_4T)4$ G-quadruplex. The band at 1136 cm^{-1} is the marker band of H_2TMPyP4 metalation; the decrease in the intensity indicates the metalation of H_2TMPyP4, because this band usually vanishes when all of the H_2TMPyP4 molecules are transferred to the AgTMPyP4 form (*43*). The band at 1242 cm^{-1} is assigned to the stretching vibration of the C_m−pyr bond; the intensity change of the band may be due to the forced rotation of pyridine when H_2TMPyP4 is bound to the $(TG_4T)4$ G-quadruplex. The rotation changes the adsorption conformation of H_2TMPyP4 on the Ag surface and thus gives the weak SERS signal. The small changes of the relative intensity of other bands also reflect the decrease of the amount of H_2TMPyP4 on the Ag surface. In summary, all of these changes in the SERS intensity and shift are ascribed to the interactions between H_2TMPyP4 and the $(TG_4T)4$ G-quadruplex.

After the binding of H_2TMPyP4 to both $(G_4T_4G_4)2$ and $AG_3(T_2AG_3)_3$ G-quadruplexes, the weak bands are observed at 1188, 1214, 1334, and 1635 cm^{-1}. The band at 1334 cm^{-1} is ascribed to the stretching vibration of the N−C_α bond (*53*−*56*); its weak intensity is due to the low concentration of AgTMPyP4 in the solution. The bands at 1188, 1214, and 1635 cm^{-1} are related to the vibration of *N*-methylpyridine. Although the *N*-methylpyridine groups are still exposed to the solvent after the porphyrin core intercalation, it is difficult for *N*-methylpyridine groups to tightly adsorb on the Ag colloid surface because of the binding effect. In addition, the shifts of two bands of H_2TMPyP4 are observed after its interaction with $(G_4T_4G_4)2$ or $AG_3(T_2AG_3)_3$. The band, corresponding to the stretching vibration of the C_α−C_m bond of H_2TMPyP4, is shifted from 1001 to 1015 cm^{-1}, and another band at 1446 cm^{-1}, mainly ascribed to the stretching vibration of the C_α−C_β bond of H_2TMPyP4 (*53*−*56*), is shifted to 1455 cm^{-1}. In fact, bands at 1015 and 1455 cm^{-1} are corresponding to the bands of AgTMPyP4 (*54*) rather than those of the free-base H_2TMPyP4; thus, the two weak bands come from a small amount of AgTMPyP4 in solutions, because a large amount of H_2TMPyP4 was intercalated to G-quadruplexes. The remaining H_2TMPyP4 is dispersed on the Ag surface to form AgTMPyP4.

The Job plots obtained by the continuous variation titration show the stoichiometric ratio of 2:1, 4:1, and 4:1 for H_2TMPyP_4 binding to $(TG_4T)4$, $(G_4T_4G_4)2$, and $AG_3(T_2AG_3)_3$, respectively. However, the *n* values fitted by the linear portion of Scatchard plots at lower *r* values are smaller than those obtained by Job plots, especially for the H_2TMPyP4/$(G_4T_4G_4)2$ complex. Direct plots, a mode equivalent to the Scatchard plot, are not hyperbolas for our results; therefore, the accurate *n* values are not obtained from it. In fact, Scatchard plots are linear only for the ligand binding to independent and equivalent sites, with any curvature because of the existence of more than one type of binding site, ligand−ligand interaction, or neighbor-exclusion effect (*58*). In addition, Direct plots are sigmoidal for our results, implying that the cooperative effects are present. Thus, the binding stoichiometric numbers obtained only from the linear part of the Scatchard plot are quite approximate. Instead, the method of the continuous variation titration is applicable for cooperative ligand binding (*59*). The *n* values obtained by Job plots should be more accurate than values fitted by the linear portion of the Scatchard plot at lower *r* values.

For the parallel $(TG_4T)4$ G-quadruplex, a 2:1 stoichiometry together with SERS results identify that two porphyrin molecules stack externally on the G-tetrads located at opposite end of the G-quadruplex (Figure 9A). This is reasonable because the end stacking can be easily formed through π stacking, without the disruption to the phosphate backbones and having less steric barriers to overcome. A similar binding mode has been proposed from the crystal diffraction and molecular-modeling studies of interactions of amidoanthraquinone with parallel G-quadruplex $(TG_4T)4$ (*13*).

On the contrary, a 4:1 stoichiometric ratio was found for both H_2TMPyP4/$(G_4T_4G_4)2$ and H_2TMPyP4/$AG_3(T_2AG_3)_3$ complexes. On the basis of this stoichiometric ratio and SERS spectra, we propose that the binding might include the mixed modes of both the end stacking in loops and intercalation between adjacent base pairs. The end stacking in both diagonal and lateral loop regions is possible and can accommodate two H_2TMPyP4 molecules. Han and Wheelhouse (*17*, *18*) have predicted this binding mode for H_2TMPyP4 with the monomer-folding $AG_3(T_2AG_3)_3$ G-quadruplex. An additional two H_2TMPyP4 molecules might intercalate between each pair of successive G-tetrad planes in the G-quadruplex, as reported by Haq and co-workers (*16*). For the $AG_3(T_2AG_3)_3$ G-quadruplex in the monomer folding, a fully intercalated mode involving both loop regions and successive G-tetrad planes would match the stoichiometric ratio. We thus conclude that the two H_2TMPyP4 molecules bind to the diagonal and lateral loop regions and the other two H_2TMPyP4 molecules intercalate the two successive G-tetrad intervals (Figure 9B).

However, $(G_4T_4G_4)2$, a dimer-hairpin-folded G-quadruplex, includes five potential binding sites, i.e., two equivalent diagonal loop regions (T_4 loops) and three equivalent intervals between the planes of four G-tetrads. Therefore, according to our current results, it is difficult to assign the exact binding sites for four H_2TMPyP4 molecules. The crystal structure reported by Haider and co-workers (*14*) shows that disubstituted aminoalkylamido acridine is bound at one end of the stack of G-tetrads of the dimer-folding $(G_4T_4G_4)2$ G-quadruplex, within one of the T4 loops. We can propose two binding models for the H_2TMPyP4/$(G_4T_4G_4)2$ complex: one model is that a H_2TMPyP4 molecule binds to one of the T4 loop regions and the other three H_2TMPyP4 molecules intercalate to the three intervals between adjacent G-tetrads (Figure 9C), and another model is that two H_2TMPyP4 molecules stack in the two T4 loops and the other two molecules intercalate to the two of three intervals (parts D and E of Figure 9).

Our results are different from those reported by Anantha et al. (*22*), Han et al. (*17*, *18*), and Haq et al. (*16*). Anantha and co-workers used the buffer solution containing 100 mM KCl and 20 mM Mg^{2+}; 100 mM KCl was used in the buffer solution for Han and co-workers' experiment; but either 200 mM NaCl or 200 mM KCl was used in the experiment by Haq and co-workers. As described above, the type and concentration of cation in the buffer solution significantly affect the structure of G-quadruplexes and the binding mode of H_2TMPyP4 is also sensitive to the changes of ionic strength (*60*), which may be the major reason for the difference of results reported by different authors. In addition, in the case of the parallel G-quadruplex, we used the TG_4T sequence but the T_4G_4 sequence was used for Haq and co-workers' and Anantha and co-workers' experiments. Although both sequences contain four guanine bases, the detailed conformational difference between $(TG_4T)4$ and $(T_4G_4)4$ G-quadruplexes in the buffer solution is not well-known. Anyway, the results reported in the literature or this paper suggest that the cations in the buffer solution play an important role in ligand binding.

Effect of H_2TMPyP4 on the Structures of G-Quadruplexes. Raman bands in the region of 1150−1600 cm^{-1} are originated primarily from in-plane vibrations of base residues, intensities of which are generally sensitive to base-stacking interactions (Raman hypochromicity) (*61*). In our results, H_2TMPyP4 binding to the $(TG_4T)4$ G-quadruplex results in Raman hypochromicities at 1483 and 1587 cm^{-1}. This is due to the effective stacking interactions between the external H_2TMPyP4 and guanine bases (*61*−*63*). On the contrary, Raman hyperchromicities are observed at 1317, 1353, 1477, 1570, and 1600 cm^{-1} for the H_2TMPyP4/$(G_4T_4G_4)2$ complex and 1333, 1376, 1486, 1610, and 1653 cm^{-1} for the H_2TMPyP4/$AG_3(T_2AG_3)_3$ complex, respectively. We speculate that the intercalation of the porphyrin core between adjacent G-tetrads can lengthen the vertical distance of two bases in both G-quadruplexes, which counteracts and weakens the stacking interactions between H_2TMPyP4 and the guanine base. In addition, the bands in the Raman difference spectra are shifted to the lower wavenumbers for the H_2TMPyP4/$(G_4T_4G_4)2$ complex, while the bands in the Raman difference spectra are shifted to the higher wavenumbers for the H_2TMPyP4/$AG_3(T_2AG_3)_3$ complex, compared with those of either $(G_4T_4G_4)2$ or $AG_3(T_2AG_3)_3$ G-quadruplex. It was reported that Raman marker bands of the specific dG conformations in telomeric DNA structures occur within the 1300−1700 cm^{-1} intervals in UVRR spectra (*37*); therefore, the shifts of these bands may originate from the conformational change of G-quadruplexes. Bands at 1317 and 1333 cm^{-1} come from the shift of the 1327 cm^{-1} band, a marker band of the syn dG conformation and base stacking, and bands at 1353 and 1376 cm^{-1} come from the band at 1363 cm^{-1}, a marker band of the anti dG conformation and sensitive to base stacking. Thus, the shifts of the bands at 1327 and 1363 cm^{-1} imply the change of the dG conformation upon H_2TMPyP4 binding. In addition, the 1376 cm^{-1} band is also assigned to dT residues and is known to exhibit increased intensity with an increasing hydrophobicity of the thymine C5-CH3 environment (*61*). Therefore, for the H_2TMPyP4/$AG_3(T_2AG_3)_3$ complex, the positive peak at 1376 cm^{-1} might also reflect the increased hydrophobicity of dT residues in the TTA loops after H_2TMPyP4 intercalated in these loops.

As noted above, any changes in the position and intensity of the 1482 cm^{-1} band reflect the changes of the interaction of the N7 site. The band at 1581 cm^{-1} is similar to the 1363 cm^{-1} band and is sensitive to base stacking, and the band near 1603 cm^{-1} is a useful probe of dG N1 hydrogen-bonding interactions. These changes in the intensity and position of bands further confirm that the intercalated H_2TMPyP4 between G-tetrads causes the conformational changes in the $(G_4T_4G_4)2$ and $AG_3(T_2AG_3)_3$ G-quadruplexes.

It was reported that the classical intercalation can cause the structural perturbations of the DNA duplex with a length increase of 3.4 Å per bound drug molecule (*64*). For the porphyrin, when it intercalates between base pairs in the duplex, DNA is extended along its axis, with an average helical rise of 3.6 Å (*65*). In addition, no apparent hypochromicities of purine or pyrimidine Raman markers were observed for ethidium bromide (EB) intercalation in duplex DNA, because the intercalated EB molecule doubles the vertical separation of the bases to 6.7 Å (*66*). Thus, our results suggest that Raman hyperchromicities in the intercalative mode are due to the increase of the distance between G-tetrads upon H_2TMPyP4 binding.

CONCLUSIONS

This study shows that H_2TMPyP4 can bind to the dimer hairpin $(G_4T_4G_4)2$ and monomer-folding $AG_3(T_2AG_3)_3$ G-quadruplexes by a mixed binding mode, including both the external stacking within loop regions and intercalation between adjacent G-tetrads, whereas the two H_2TMPyP4 molecules are bound to the two ends of the parallel-stranded $(TG_4T)4$ G-quadruplex. The intercalation in the successive G-tetrads and loop regions indicates that the adjacent repulsion is not significant. Our results present the apparent disparity with the reported binding modes that reveals the complexity of H_2TMPyP4/G-quadruplexes binding behaviors. The external stacking of H_2TMPyP4 does not change the structure of the $(TG_4T)4$ G-quadruplex, and a significant stacking effect (Raman hypochromicities) is observed. Instead, the intercalative H_2TMPyP4 molecules lead to Raman hyperchromicities and shifts of $(G_4T_4G_4)2$ and $AG_3(T_2AG_3)_3$ G-quadruplexes, suggesting that the intercalative H_2TMPyP4 molecules lengthen the vertical distance between base pairs and affect the structures of $(G_4T_4G_4)2$ and $AG_3(T_2AG_3)_3$ G-quadruplexes. These results further provide new insight into the structural change of G-quadruplexes upon H_2TMPyP4 binding.

SUPPORTING INFORMATION AVAILABLE

Absorption difference spectra for H_2TMPyP4 with the different G-quadruplexes used to generate Job plots (Figure S1). This material is available free of charge via the Internet at http://pubs.acs.org.

REFERENCES

1. Haider, S., Parkinson, G. N., and Neidle, S. (2002) Crystal structure of the potassium form of an *Oxytricha nova* G-quadruplex, *J. Mol. Biol. 320*, 189−200.
2. Cech, T. R. (2000) Life at the end of the chromosome: Telemeres and telomerase, *Angew. Chem., Int. Ed. 39*, 34−43.
3. Neidle, S., and Parkinson, G. N. (2003) The structure of telomeric DNA, *Curr. Opin. Struct. Biol. 13*, 275−283
4. Simonsson, T. (2001) G-quadruplex DNA structures−Variation on a theme, *Biol. Chem. 382*, 621−628.
5. Keniry, M. A. (2001) Quadruplex structures in nucleic acids, *Biopolymers 56*, 123−146.
6. Rezler, E. M., Bearss, D. J., and Hurley, L. H. (2002) Telomeres and telomerase as drug targets, *Curr. Opin. Pharmacol. 2*, 415−423.
7. Neidle, S., and Parkinson, G. (2002) Telomere maintenance as a target for anticancer drug discovery, *Nat. Rev. Drug Discovery 383*, 383−393.
8. Fedoroff, O. Y., Salazar, M., Han, H., Chemeris, V. V., Kerwin, S. M., and Hurly, L. H. (1998) NMR-based model of a telomerase-inhibiting compound bound to G-quadruplex DNA, *Biochemistry 37*, 12367−12374.
9. Han, H., and Hurley, L. H. (2000) G-quadruplex DNA: A potential target for anti-cancer drug design, *Trends Pharmacol. Sci. 21*, 136−141.
10. Randazzo, A., Galeone, A., and Luciano, M. (2001) ^{1}H-NMR study of the interaction of distamycin A and netropsin with the parallel stranded tetraplex [d(TGGGGT)]4, *Chem. Commun.* 1030−1031.
11. Gavathiotis, E., Heald, R. A., Stevens, M. F. G., and Searle, M. S. (2003) Drug recognition and stabilization of the parallel-stranded DNA quandruplex d(TTAGGGT)4 containing the human telomeric repeat, *J. Mol. Biol. 334*, 25−36.
12. Clark, G. R., Pytel, P. D., Squire, C. J., and Neidle, S. (2003) Structural of the first parallel DNA quadruplex−drug complex, *J. Am. Chem. Soc. 125*, 4066−1067.
13. Read, M. A., and Neidle, S. (2000) Structural characterization of a guanine-quadruplex ligand complex, *Biochemistry 39*, 13422−13432.
14. Haider, S. M., Parkinson, G. N., and Neidle, S. (2003) Structure of a G-quadruplex−ligand complex, *J. Mol. Biol. 326*, 117−125.
15. Anantha, N. V., Azam, M., and Sheardy, R. D. (1998) Porphyrin binding to quadruplexed T_4G_4, *Biochemistry 37*, 2709−2714.
16. Haq, I., Trent, J. O., Chowdhry, B. Z., and Jenkins, T. C., (1999) Intercalative G-tetraplex stabilization of telomeric DNA by a cationic Porphyrin, *J. Am. Chem. Soc. 121*, 1768−1779.
17. Han, H., Langley, D. R., Rangan, A., and Hurley, L. H., (2001) Selective interactions of cations porphyrins with G-quadruplex structures, *J. Am. Chem. Soc. 123*, 8902−8913.
18. Wheelhouse, R. T., Sun, D., Han, H., Han, F. X., and Hurley L. H. (1998) Cationic porphyrins as telomerase inhibitors: The interaction of tetra-(*N*-methyl-4-pyridyl) porphine with quadruplex DNA, *J. Am. Chem. Soc. 120*, 3261−3262.
19. Wheelhouse, R. T., Sun, D., Han, H., Han, F. X., and Hurley L. H. (1999) Interactions of TMPyP4 and TMPyP2 with quadruplex DNA. Structural basis for the differential effects on telomerase inhibition, *J. Am. Chem. Soc. 121*, 3561−3570.
20. Dixon, I. M., Lopez, F., Estève, J.-P., Blasco, T. M. A., Pratviel, G., and Meunier, B. (2005) Porphyrin derivatives for telomere binding and telomerase inhibition, *ChemBioChem 6*, 123−132.
21. Keating, L. R., and Szalai, V. A. (2004) Parallel-stranded guanine quadruplex interactions with a copper cationic porphyrin, *Biochemistry 43*, 15891−15900.
22. Anantha, N. V., Azam, M., and Sheardy, R. D. (1998) Porphyrin binding to quadruplexes T_4G_4, *Biochemistry 37*, 2709−2714.
23. Izbicka, E., Wheelhouse, R.T., Raymond, E., Davidson, K. K., Lawrence, R. A., Sun, D., Windle, B. W., Hurley, L. H., and von Hoff, D. D. (1999) Effects of cationic porphyrins as G-quadruplex intercative angents in human tumor cells, *Cancer Res. 59*, 639−644.
24. Pasternack, R. F., Gibbs, E. J., and Villaffranca, J. J. (1983) Interactions of porphyrins with nucleic acids, *Biochemistry 22*, 2406−2414.
25. Cantor, C. R., Warshaw, M. W., and Shapiro, H. (1970) Oligonucleotide interactions. III. Circular dichroism studies of the conformation of deooxyoligonucleotides, *Biopolymers 9*, 1059−1077.
26. Chaires, J. B. (2001) Analysis and interpretation of ligand−DNA binding isotherms, *Methods Enzymol. 340*, 3−22.
27. Cantor, C. R., and Schimmel, P. R. (1980) *Biophysical Chemistry*, Vol. 2, W. H. Freeman, San Fransisco, CA.
28. Likussar, W., and Blotz, D. F. (1971) Theory of continuous variations plots and a new method for spectrophotometric determination of extraction and formation constants, *Anal. Chem. 43*, 1265−1272.
29. Ingham, K. C. (1975) On the application of Job's method of continuous variation to the stoichiometry of protein−ligand complexes, *Anal. Biochem. 68*, 660−663.
30. Lee, P. C., and Meisel, D. (1992) Adsorption and surface-enhanced Raman of dyes on silver and gold sols, *J. Phys. Chem. 86*, 3391−3395.
31. He, X., Ding, Y., Li, D., and Lin, B. (2004) Recent advances in biomelocular interactions by capillary electrophoresis, *Electrophoresis 25*, 697−711.
32. De Groot, J., and Hester, R. E. (1987) Surface-enhanced resonance Raman spectroscopy of oxyhemoglobin adsorbed onto colloidal silver, *J. Phys. Chem. 91*, 1693−1696.
33. Rodriguez-Mendieta, I. R., Spence, G. R., Gell, C., Radford, S. E., and Smith, D. A. (2005) Ultraviolet resonance Raman studies reveal the environment of tryptophan and tyrosine residues in the native and partially folded states of the E colicin-binding immunity protein Im7, *Biochemistry 44*, 3306−3315.
34. Fodor, S. P. A., Rava, R. P., Hays, T. R., and Spiro, T. G. (1985) Ultraviolet resonance Raman spectroscopy of the nucleotides with 266-, 240-, 218-, and 200-nm pulsed laser, *J. Am. Chem. Soc. 107*, 1520−1529.
35. Laporte L., and Thomas, G. J., Jr. (1998) A hairpin conformation for the 3′ overhang of *Oxytricha nova* telomeric DNA, *J. Mol. Biol. 281*, 261−270.
36. Miura, T., and Thomas, G. J., Jr. (1995) Structure and dynamics of interstrand guanine association in quadruplex telomeric DNA, *Biochemistry 34*, 9645−9654.
37. Krafft, C., Benevides, J. M., and Thomas, G. J., Jr. (2002) Secondary structure polymorphism in *Oxytricha nova* telomeric DNA, *Nucleic Acids Res. 30*, 3981−3991.
38. Benevides, J. M., Overman, S. A., and Thomas, G. J., Jr. (2005) Raman, polarized Raman and ultraviolet resonance Raman

spectroscopy of nucleic acids and their complexes, *J. Raman Spectrosc. 36*, 279−299.
39. Laughlan, G., Murchie, A. I. H., Norman, D. G., Moore, M. H., Moody, P. C. E., Lilley, D. M. J., and Luisi, B. (1994) The high-resolution crystal structure of a parallel-stranded guanine tetraplex, *Science 265*, 520−524.
40. Philips, K., Dauter, Z., Murchie, A. I. H., Lilly, D. M. J., and Luisi, B. (1997) The crystal structure of a parallel-stranded guanine tetraplex at 0.95 Å resolution, *J. Mol. Biol. 273*, 171−182.
41. Wang, Y., and Patel, D. J. (1993) Solution structure of the human telomeric repeat d[$AG_3(T_2AG_3)_3$] G-tetraplex, *Structure 1*, 263−282.
42. Schultze, P., Smith, F. W., and Feigon, J. (1994) Refined solution structure of the dimmer quadruplex formed from the *Oxytricha* telomeric oligonucleotide d(GGGGTTTTGGGG), *Structure 2*, 221−233.
43. Smith, F. W., and Feigon, J. (1992) Quadruplex structure of *Oxytricha* telomeric DNA oligonucleotides, *Nature 356*, 164−168.
44. Dougherty, G., Pilbrow, J. R., Skorobogaty, A., and Smith, T. D. (1985) Electron spin resonance spectroscopic and spectrophotometric investigation of the binding of the tetracationic porphyrins and porphyrazines with calf thymus DNA, *J. Chem. Soc., Faraday Trans. 81*, 1739−1759.
45. Smith, F. W., and Feigon, J. (1993) Strand orientation in the DNA quadruplex formed from the *Oxytricha* telomere repeat oligonucleotide d($G_4T_4G_4$) in solution, *Biochemistry 32*, 8682−8692.
46. Schultze, P., Smith, F. W., and Feigon, J. (1994) Refined solution structure of the dimeric quadruplex formed from the *Oxytricha* telomeric olignucleotide d(GGGGTTTTGGGG), *Structure 2*, 221−223.
47. Kang, C., Zhang, X., Ratliff, R., Moyzis, R., and Rich, A. (1992) Crystal structure of four-stranded *Oxytricha* telomeric DNA, *Nature 356*, 126−131.
48. Li, W., Wu, P., Ohmichi, T., and Sugimoto, N. (2002) Characterization and thermodynamic properties of quadruplex/duplex competition, *FEBS Lett. 526*, 77−81.
49. Parkinson G. N., Lee, M. P. H., and Neidle, S. (2002) Crystal structure of parallel quadruplexes from human telomeric DNA, *Nature 417*, 876−880.
50. Makarska, M., Radzki, St., and Legendziewicz, J. (2002) Spectroscopic characterixation of water-soluble cationic porphyrins and their complexes with Cu(II) in various solvents, *J. Alloys Compd. 341*, 233−238.
51. Zupán, K., Hérenyi, L., Tóth, K., Maier, Z., and Csík, G. (2004) Binding of cationic porphyrin to isolated and encapsidated viral DNA analyzed by comprehensive spectroscopic methods, *Biochemistry 43*, 9151−9159.
52. Breuzard, G., Millot, J.-M., Riou, J.-F., and Manfait, M. (2003) Selective interactions of ethidiums with G-quadruplex DNA revealed by surface-enhanced Raman scattering, *Anal. Chem. 75*, 4305−4311.
53. Hanzlíková, J., Procházka, M., Štěpánek, J., Bok, J., Baumruk, V., and Anzenbacher, P. Jr. (1998) Metalation of 5,10,15,20-tetrakis(1-methyl-4-pyridyl) porphyrin in silver colloids studied via time dependence of surface-enhancec resonance Raman spectra, *J. Raman Spectrosc. 29*, 575−584.
54. Blom, N., Odo, J., and Nakamoto, K. (1986) Resonance Raman studies of metal tetrakis(4-*N*-methylpyridyl) porphine: Band assignments, structure-sensitive bands, and species equilibria, *J. Phys. Chem. 90*, 2847−2852.
55. Terekhov, S. N., Kruglik, S. G., Malinovskii, V. L., Galievsky, V. A., Chirvony, V. S., and Turpin, P.-Y. (2003) Resonance Raman characterization of cationic Co(II) and Co(III) tetrakis(*N*-methyl-4-pyridinyl) porphyrins in aqueous and non-aqueous media, *J. Raman Spectrosc. 34*, 868−881.
56. Schneider, J. H., Odo, J., and Nakamoto, K. (1988) Interaction of water-soluble metalloporphyrins with nucleic acids by resonance Raman spectroscopy, *Nucleic Acids Res. 16*, 10323−10338.
57. Procházka, M., Turpin, P.-Y., Štěpánek, J., and Bok, J. (1999) Metallation kinetics of a free base porphyrin in surface-enhanced resonance Raman scattering active Ag colloid system as a probe of porphyrin−nucleic acids interaction, *J. Mol. Struct. 482−483*, 221−224.
58. McGhee, J. D., and von Hippel, P. H. (1974) Theoretical aspects of DNA-protein interactions: Co-operative and non-co-operative binding of large ligands to a one-dimensional homogeneous lattice, *J. Mol. Biol. 86*, 469−489.
59. Huang, C. Y. (1982) Determination of binding stoichiometry by the continuous variation method: The Job plot, *Methods Enzymol. 87*, 509−525.
60. Pasternack, R. F., and Gibbs, E. J. (1989) Interactions of porphyrins and metalloporphyrins with nucleic acids, in *Metal−DNA Chemistry* (Tullius, T., Ed.) pp 59−73, American Chemical Society, Washington, DC.
61. Deng, H., Bloomfield, V. A., Benevides, J. M., and Thomas, G. J., Jr. (1999) Dependence of the Raman signature of genomic B-DNA on nucleotide base sequence, *Biopolymers 50*, 656−666.
62. Movileanu, L., Benevides, J. M., and Thomas, G. J., Jr. (2002) Temperature dependence of the Raman spectrum of DNA. I. Raman signatures of premelting and melting transitions of poly(dA-dT)·poly(dA-dT), *J. Raman Spectrosc. 30*, 637−649.
63. Wen, Z. Q., and Thomas, G. J., Jr. (1998) UV resonance Raman spectroscopy of DNA and protein constituents of viruses: Assignments and cross sections for excitations at 257, 244, 238, and 229 nm, *Biopolymer 45*, 247−256.
64. Haq, I., and Ladbury, J. (2000) Drug−DNA recognition: Energetics and implications for design, *J. Mol. Recognit. 13*, 188−197.
65. Lipscomb, L. A., Zhou, F. X., Presnell, S. R., Woo, R. J., Peek, M. E., Plaskon, R. R., and Williams, L.D. (1996) Structure of a DNA−porphyrin complex, *Biochemistry 35*, 2818−2823.
66. Benevides, J. M., and Thomas, G. J., Jr. (2005) Local conformational changes induced in B-DNA by ethidium intercalation, *Biochemistry 44*, 2993−2999.

BI052356Z